Available online at www.sciencedirect.com

SciVerse ScienceDirect

journal homepage: www.elsevier.com/locate/watres

Optimization of salt adsorption rate in membrane capacitive deionization

R. Zhao [a,b,*], O. Satpradit [b], H.H.M. Rijnaarts [a], P.M. Biesheuvel [a,b], A. van der Wal [a]

[a] Department of Environmental Technology, Wageningen University, Bornse Weilanden 9, 6708 WG Wageningen, The Netherlands
[b] Wetsus, Centre of Excellence for Sustainable Water Technology, Agora 1, 8934 CJ Leeuwarden, The Netherlands

ARTICLE INFO

Article history:
Received 15 September 2012
Received in revised form
9 January 2013
Accepted 13 January 2013
Available online 24 January 2013

Keywords:
Membrane capacitive deionization
Ion exchange membrane
Desalination
Water recovery
Salt adsorption rate
Porous electrode model
Constant current operation
Constant voltage operation

ABSTRACT

Membrane capacitive deionization (MCDI) is a water desalination technique based on applying a cell voltage between two oppositely placed porous electrodes sandwiching a spacer channel that transports the water to be desalinated. In MCDI, ion-exchange membranes are positioned in front of each porous electrode to prevent co-ions from leaving the electrode region during ion adsorption, thereby enhancing the salt adsorption capacity. MCDI can be operated at constant cell voltage (CV), or at a constant electrical current (CC).

In this paper, we present both experimental and theoretical results for desalination capacity and rate in MCDI (both in the CV- and the CC-mode) as function of adsorption/desorption time, salt feed concentration, electrical current, and cell voltage. We demonstrate how by varying each parameter individually, it is possible to systematically optimize the parameter settings of a given system to achieve the highest average salt adsorption rate and water recovery.

1. Introduction

Lack of access to fresh water is one of the most severe issues for humanity in the 21st century (Cipollina, 2009). Two-third of the world population will be facing water scarcity by 2025 (Buerkle, 2007). Desalination technologies are used to generate fresh water from sea water and brackish water. The state-of-the-art desalination technology, namely Reverse Osmosis (RO), extracts fresh water from salt water by pressurizing the feed water on one side of a semi-permeable membrane. RO is considered to be energy-efficient for treating high salinity streams. However, to treat streams with lower salt concentration, say below ~5000 ppm, RO becomes relatively less efficient (Anderson et al., 2010; Cipollina, 2009). To treat brackish water, Capacitive Deionization (CDI) serves as an efficient alternative, which extracts the ions from the feed solution instead of extracting the water. A CDI cell consists of two conductive porous electrodes, which are materials with a high internal surface area around ~1000 m^2/g, two graphite current collectors that facilitate electron transport in and out of the electrodes, and a spacer channel in between the electrodes for the transport of the water, see Fig. 1. In a practical CDI unit, several parallel cells are assembled into one stack. When an electrical voltage is applied across the cell, ions in the spacer channel are transported towards the electrodes and adsorb in the electrical double layers (EDLs) formed

* *Corresponding author*. Department of Environmental Technology, Wageningen University, Bornse Weilanden 9, 6708 WG Wageningen, The Netherlands. Tel.: +317483339.
E-mail address: ran.zhao@wetsus.nl (R. Zhao).
0043-1354/$ – see front matter © 2013 Elsevier Ltd. All rights reserved.
http://dx.doi.org/10.1016/j.watres.2013.01.025

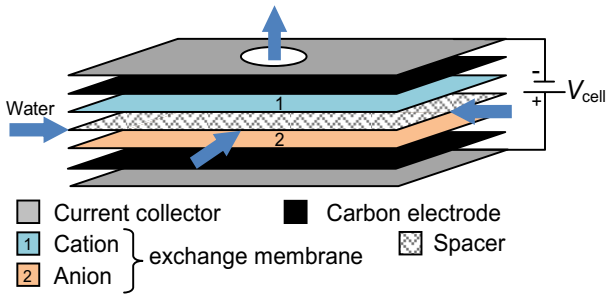

Fig. 1 – Schematic view of the membrane capacitive deionization (MCDI) process. Influenced by an applied electrical field, cations in the water flowing through the spacer channel migrate through the cation-exchange membrane and are stored inside the adjacent porous electrode; simultaneously, anions are stored in the opposite electrode.

within the micropores in the porous electrode structure (Arnold and Murphy, 1961; Avraham et al., 2011; Haro et al., 2011; Humplik et al., 2011; Seo et al., 2010; Suss et al., 2012; Zou et al., 2010).

A Membrane Capacitive Deionization (MCDI) cell has a similar configuration as a conventional CDI cell, but in addition contains anion and cation-exchange membranes which are positioned between the spacer channel and the anode, and between the spacer channel and the cathode, respectively (Biesheuvel et al., 2011b; Kim et al., 2010; Kim and Choi, 2010; Lee et al., 2006, 2011; Li et al., 2008; Li and Zou, 2011; Nie et al., 2011; Park et al., 2011), see Fig. 1. It is also possible to use only one membrane, in front of only one electrode (Kim and Choi, 2010; Porada et al., 2012a). Because the membranes block transport of co-ions, the macropores within the electrode structure become available as extra storage space for ions, and MCDI can remove more salt than CDI (Biesheuvel et al., 2011b; Porada et al., 2012b; Zhao et al., 2012a). The exact mechanism of ion adsorption in CDI and MCDI will be explained in detail in the theory section.

So far, the overwhelming majority of CDI and MCDI research has focused on applying a constant cell voltage (CV) between the electrodes during the adsorption step, followed by short-circuiting of the electrodes, or reversing the voltage, during the desorption step. Recently it has been demonstrated that in MCDI charging and discharging the electrodes at constant current (CC) can have several major advantages in comparison with CV, such as a constant (i.e., not varying in time) and adjustable effluent concentration (Zhao et al., 2012a).

For all desalination technologies, it is essential to maximize the desalination performance, i.e., the extent of desalination per unit time, besides optimizing the water recovery (WR), which is the ratio of the flow of freshwater relative to the flow of feed water. In the present manuscript, we focus exclusively on MCDI and analyse the influence of several process parameters such as adsorption time, water flowrate, and adsorption current, to investigate the influence of each parameter on two key performance indicators in MCDI, namely the average salt adsorption rate (ASAR) and water recovery, WR. We discuss both the CC operational mode, as well as CV operation. The aim of our work is to demonstrate how the average salt adsorption rate and the water recovery can be systematically optimized for a given MCDI system.

2. Materials and methods

Experimental details of the MCDI stack design used in this work have been outlined previously (Biesheuvel et al., 2011b; Porada et al., 2012b; Zhao et al., 2010) and will be briefly summarized here. Materials used are graphite current collectors (thickness $\delta = 250$ μm), porous carbon electrodes (Materials & Methods LLC., PACMM™ 203, Irvine, CA, $\delta_e = 362$ μm, anion and cation-exchange membranes (Neosepta AMX, $\delta_{mem} = 140$ μm, and Neosepta CMX, $\delta_{mem} = 170$ μm, Tokuyama, Japan) and a polymer spacer (Glass fibre prefilter, Millipore, Ireland, $\delta_{sp} = 250$ μm). In the MCDI stack, we use $N = 8$ cells, with total electrode mass of 10.8 g. The salt solution flows from all four sides of the stack into the square 6·6 cm^2 spacer channel of each of the N cells, and leaves from a hole (1.5·1.5 cm^2) in the middle of each cell. After assembly, all layers in the stack are compressed and placed in a PTFE housing. The stack is fed from a 10 L vessel with NaCl as the electrolyte, to which the effluent is recycled. The conductivity of the effluent of the stack is measured in-line and is converted into salt concentration according to a calibration curve. Effluent pH is also measured and used to correct the measured conductivity. The electrical current through the cell is applied using a potentiostat (Iviumstat standard, Ivium Technologies, The Netherlands) which can simultaneously apply and measure the cell voltage and the electrical current between the two electrodes. Reference electrodes are not used in our experiments.

In this paper, experimental and theoretical work of MCDI is reported as function of several input parameters. In the experiments, we vary each of them in turn, while keeping the others at their reference settings, see Tables 1 and 2. For constant current operation (CC), the reference settings for the whole stack are defined as follows: during ion adsorption we apply an electrical current of 1 A to the entire stack, until the cell voltage reaches $V_{cell} = 1.6$ V. At this moment we switch from the ion adsorption step to the ion desorption step by changing either the voltage or the current. Note that an electrical current of 1 A is equal to a current density of ~37 A per m^2 electrode area. During desorption, we either immediately switch off the cell voltage to $V_{cell} = 0$ V for a fixed period of time (500 s) (as if short-circuiting the cell), which is the zero-volt desorption mode (ZVD), see Table 1, or we apply

Table 1 – Reference settings for MCDI-CC operation in ZVD mode.

Influent salt concentration (NaCl)	20 mM
Adsorption current (applied until the cell voltage reaches $V_{cell} = 1.6$ V)	1 A (~37 A/m^2)
Water flowrate (stack)	60 mL/min
Desorption time	500 s

Table 2 – Reference settings for MCDI-CC operation in RCD mode. Except for desorption current, all settings are fixed throughout Section 4.1.2.

Influent salt concentration (NaCl)	20 mM
Adsorption current (applied until the cell voltage increases to $V_{cell} = 1.6$ V)	1 A (~37 A/m^2)
Water flowrate (stack)	60 mL/min
Desorption current (applied until the cell voltage decreases to 0 V)	−0.2 to −2 A

an electrical current of −1 A until the cell voltage drops back to 0 V, which is the reverse-current desorption mode (RCD), see Table 2. The ZVD and the RCD mode will be discussed in Section 4.1.1 and 4.1.2. Note that in these experiments for CC-RCD operation of MCDI, only one input parameter, namely the desorption current, is varied in the range of −0.2 A and −2 A, while the other input parameters are unchanged, see Table 2 and Fig. 5.

For constant voltage operation (CV), we define the reference settings as follows: A cell voltage of $V_{cell} = 1.2$ V is applied during ion adsorption for 500 s, and during ion desorption, we either immediately drop the cell voltage to $V_{cell} = 0$ V for a fixed duration of 500 s, which is the zero-volt desorption mode (ZVD), or we apply a reversed voltage of −1.2 V, again for 500 s, which is the reverse-voltage desorption mode (RVD). These two reference settings for CV were defined in our previous work as 0-MCDI and r-MCDI, respectively (Biesheuvel et al., 2011b). A full cycle consist of an ion adsorption step followed by an ion desorption step. During both steps of the cycle, a 20 mM NaCl solution is continuously pumped into the stack at a constant water flowrate of 60 mL/min for the whole stack, which is equal to 7.5 mL/min per cell. The effluent is recycled back to the reservoir (solution residence time in reservoir ~3 h).

The salt adsorption and charge in an MCDI-cycle can be derived from the data of the salt effluent (outflow) concentration versus time, and from the data for electrical current versus time, respectively, following the procedures as explained by Zhao et al. (2010) and Biesheuvel et al. (2011b). For salt adsorption, the difference in inflow salt concentration and outflow concentration is integrated with regard to time, and multiplied with the water flowrate, while for charge, the current is integrated over time. The dynamic steady state (DSS) is reached after a few cycles, when the measured salt adsorption during one phase of the cycle is equal to the salt desorption in the other phase of the cycle (salt balance is maintained). Likewise in the DSS, the total electrical charge transferred in one direction (from cathode to anode) during the adsorption step, is equal to that transferred in the opposite direction during the desorption step except for a small leakage current. After start of a new experiment (new settings) it takes a few cycles to reach the dynamic steady-state (DSS) (Biesheuvel et al., 2011b). All data shown in this manuscript are obtained under the DSS condition.

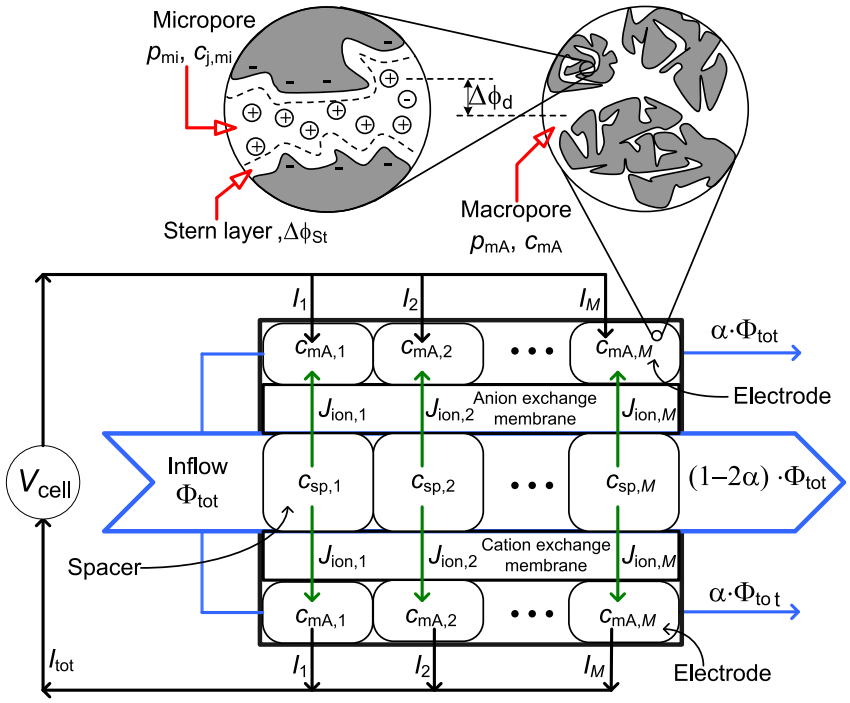

Fig. 2 – Schematic view of MCDI model for ion transport and storage. Φ_{tot} is the total water flowrate per cell. The fraction of that which runs inadvertently through each of the electrodes is α. $J_{ion,i}$ is the ion flux from spacer channel into the electrode for each of the $i = 1...M$ mathematical sub-cells that are placed in series in the model. I_i ($i = 1...M$) is the electrical current density for each sub-cell, and I_{tot} is the total average ion current density. V_{cell} is the voltage drop across the cell between two electrodes. In the electrode, macropores and micropores co-exist. In the macropores cations and anions have the same concentration c_{mA}, while in the micropores the difference between cation and anion number is balanced by the electrical charge present in the carbon matrix.

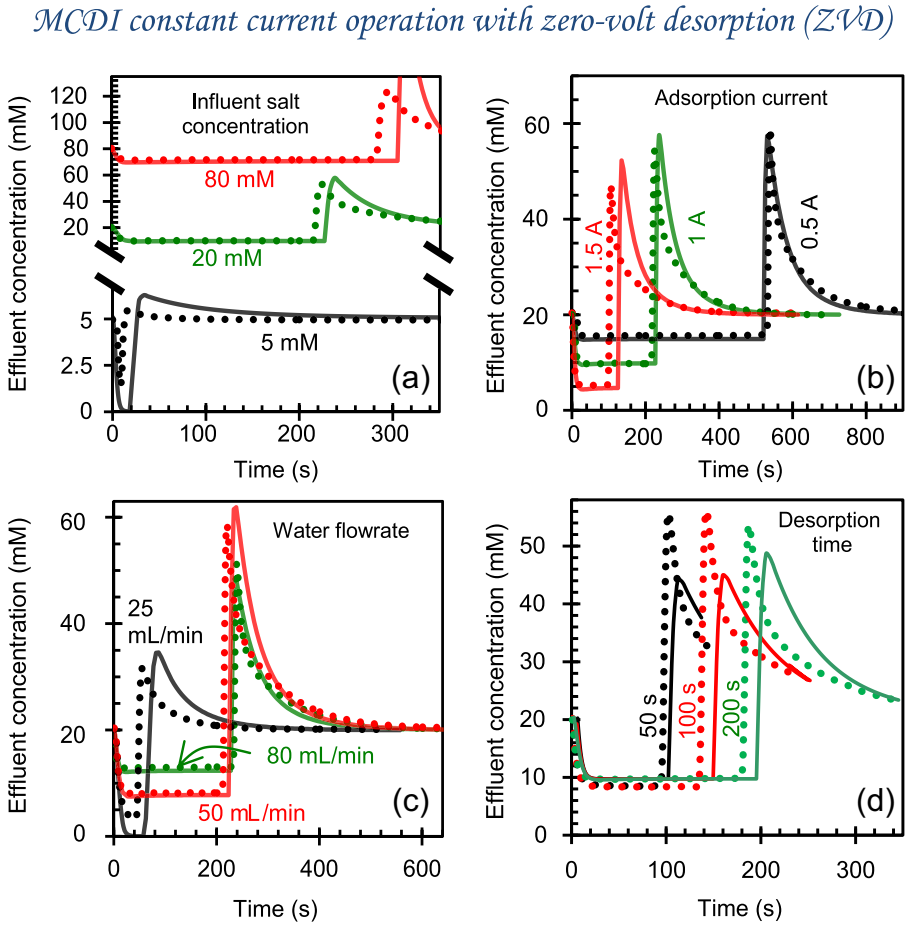

Fig. 3 – Effluent salt concentration during a dynamic steady-state cycle for CC-MCDI in ZVD-mode as function of experimental parameters varied around the reference settings, see Table 1: (a) influent salt concentration, (b) adsorption current, (c) water flowrate, and (d) desorption time. The dotted lines are experiments, and the solid lines are theory.

3. Theory

To describe the desalination performance of MCDI, we use a theoretical model for the MCDI process that takes into account many geometrical and experimental details. To describe ion adsorption in the porous electrode during capacitive charging, we use the two-porosity model that considers the two types of porosity in the electrodes, namely the macropores (transport pathways) in between the porous activated carbon particles, and the micropores (intraparticle porosity) within the carbon particles, see Fig. 2 (Biesheuvel et al., 2011a, 2011b; 2012; Porada et al., 2012c; Zhao et al., 2012b). In MCDI, after an electrical current or voltage is applied, counterions will pass through the membrane into the electrode, and move via the macropores into the micropores, where they will be stored in the electrical double layers (EDLs). Simultaneously, co-ions are expelled from the micropores, but are prevented from leaving the electrode region because of the ion-exchange membranes placed in front of the electrodes; these ions will therefore end up in the macropores of the electrode. Because the macropores are always electrically neutral (which implies that the amount of co-ions there equals the amount of counterions), additional counterions can migrate from the spacer channel into the macropores, thereby enlarging the salt storage capacity when membranes are used, i.e., when MCDI is used instead of CDI. These effects of micro- and macropores, and the membrane, are included in the present model. In the model we describe the plug-flow character of the spacer channel by placing a certain number (M) of ideally stirred volumes, or 'sub-cells' in series.

3.1. *Electrostatic double layers in porous electrodes and overall cell voltage balance*

In the two-porosity model (Biesheuvel et al., 2011b), the transport of ions across the electrode takes place through the macropores which form the space in between the carbon particles (typical dimension of the order of one to several μm) with porosity of p_{mA} (macropore volume per unit total electrode volume). The micropores are where the counterions are preferentially stored in the electrical double layers (EDLs). The pore size of the micropores is typically a few nanometres or less.

In the macropores, c_{cation} has the same concentration as c_{anion} and thus a salt concentration c_{salt} (per unit of macropore volume) can be defined. Micropores are the pores inside the carbon particles, which have a porosity of p_{mi} (micropore volume per unit total electrode volume), in which the

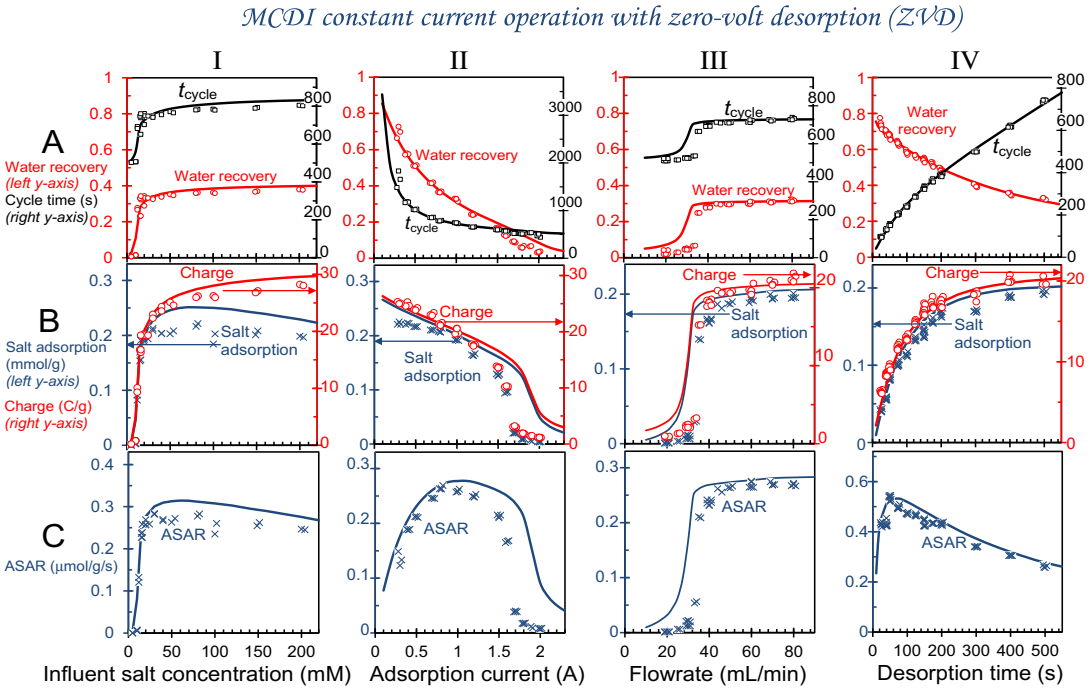

Fig. 4 – Experimental and theoretical results for operation of MCDI-CC in ZVD-mode. Water recovery and total cycle time (t_{cycle}) (row A), salt adsorption and charge per cycle, per gram of total electrode mass (row B), and average salt adsorption rate (ASAR) (row C). Each column describes the results based on varying one input parameter at a time: column I influent salt concentration, column II adsorption current, column III water flowrate, and column IV desorption time. Symbols are experimental data, and lines are theory. Reference settings are given in Table 1.

cation concentration, $c_{cation,mi}$ can differ from the anion concentration, $c_{anion,mi}$ (ion concentration per unit of micropore volume). As the size of the micropores is smaller than the Debye length (a length scale to characterize the thickness of the diffuse part of the double layer in the classical Gouy–-Chapman–Stern theory for a single double layer), the EDLs will overlap strongly. This allows us to use the Donnan approach of assuming a constant electrostatic potential in the micropore space relative to that in the macropores, $\Delta\phi_d$, and to relate the ion concentration in the micropores to that in the macropores according to

$$c_{j,mi} = c_{mA} \cdot \exp\left(-z_j \cdot \Delta\phi_d + \mu_{att}\right), \quad (1)$$

where $z_j = +1$ for the cation and $z_j = -1$ for the anion, and where μ_{att} is an attractive term which quantifies the chemical attraction between ions and the carbon material. In order to keep symmetry and simplicity in the present model, we will use the same value of μ_{att} for both the cation (Na^+) and the anion (Cl^-), though in a generalized model this assumption can be relaxed. In Eq. (1), $\Delta\phi_d$ is the Donnan potential difference between inside (micropores) and outside (macropores) of the porous carbon particles.

Inside the micropores, the difference between $c_{cation,mi}$ and $c_{anion,mi}$ is defined as the 'charge concentration', $c_{charge,mi} = c_{cation,mi} - c_{anion,mi}$. This charge, $c_{charge,mi}$, relates to the potential difference across a Stern layer, $\Delta\phi_{St}$, which is located in between the water-filled micropores and the carbon matrix, in accordance with the Gauss equation,

$$c_{charge,mi} \cdot F = -V_T \cdot \Delta\phi_{St} C_{St,vol}, \quad (2)$$

where F is the Faraday constant (96,485 C/mol), V_T is the thermal voltage ($=RT/F \sim 25.7$ mV at room temperature), and $C_{St,vol}$ is the volumetric capacitance of the Stern layer. For the Stern capacity, $C_{St,vol}$, we use the empirical expression $C_{St,vol} = C_{St,vol,0} + \alpha \cdot c^2_{charge,mi}$ which makes $C_{St,vol}$ go up slightly with micropore charge. The charge concentration also relates to the current density I (per projected area of the electrode, A) by

$$\delta_{elec} \cdot \frac{\partial}{\partial t}\left(p_{mi} \cdot c_{charge,mi}\right) = I, \quad (3)$$

where δ_{elec} is the electrode thickness and t is time. At this point it is relevant to note that Eqs. (1)–(11) in Section 3.1 and 3.2 are solved separately for each sub-cell. For instance, the current density I_i (used e.g. in Eq. (3) above) is calculated for each sub-cell separately, with the total average current density I_{tot} given by $I_{tot} = 1/M \sum_{i=1}^{M} I_i$. Important is that the total cell voltage difference V_{cell}, see Eq. (5), is at each moment in time the same for each sub-cell, although it changes in time for CC operation.

The description of ion transport through the porous electrodes is a complicated problem (Biesheuvel et al., 2011a, 2012; Rica et al., 2012; Zhao et al., 2012b). Here we follow a simplified approach, and do not describe ion transport in the electrode in detail. We do, however, in an empirical way include an electrode resistance, via an electrode voltage drop, $\Delta\phi_{elec}$, which depends on current and macropore ion concentration (high

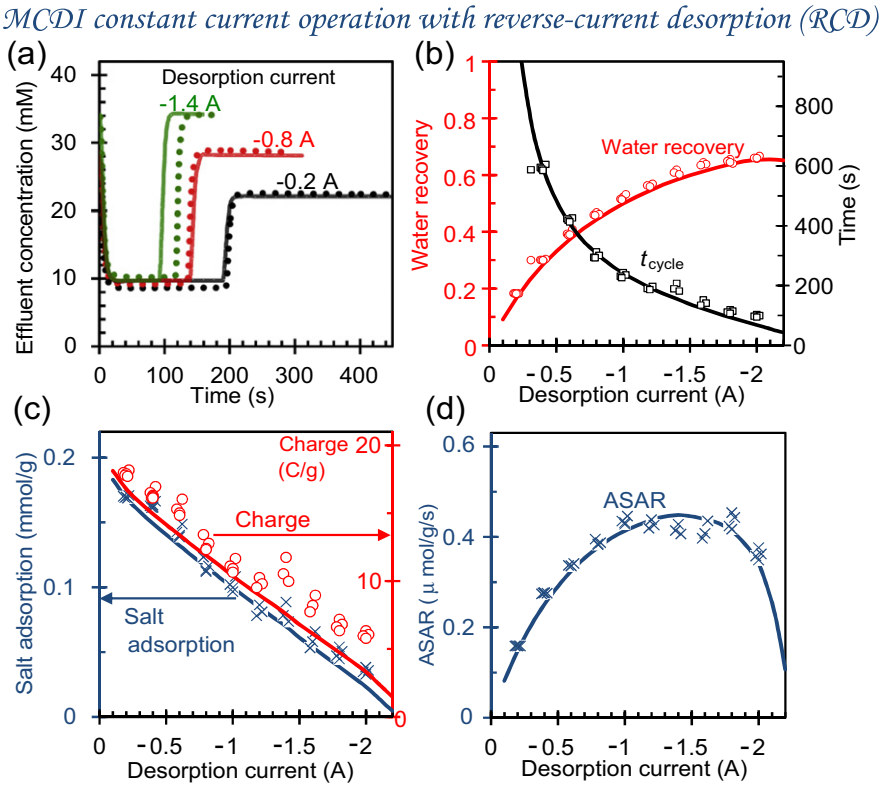

Fig. 5 – Experimental and theoretical results for MCDI-CC operation in RCD mode. (a) Effluent salt concentration as function of time during one cycle. Dotted lines: experiments, solid lines: theory. (b) Water recovery and total cycle time. (c) Salt adsorption and charge per cycle per gram total electrode mass. (d) Average salt adsorption rate (ASAR). For panels (b), (c) and (d) symbols are experimental data and lines are theory. See Table 2 for reference settings.

concentrations lead to a low voltage drop). Using this approach, the current I relates to the electrode potential drop, $\Delta\phi_{elec}$, according to

$$\Delta\phi_{elec}\cdot V_T = -I\cdot F\cdot R_{elec}/c_{mA}, \tag{4}$$

where R_{elec} is an electrode specific resistance with dimension Ω mol/m.

The cell is assumed to be symmetrical as we use a simple 1:1 salt, NaCl, as the electrolyte and take equal values for porosities p, Stern capacity $C_{St,vol}$, and chemical attraction μ_{att}, for both electrodes. Thus the voltage drop across the cell between the two electrodes is given by

$$\begin{aligned}\frac{1}{2}V_{cell}/V_T = {} & \Delta\phi_{sp,half} + \Delta\phi_{donnan,membrane/spacer} + \Delta\phi_{mem} \\ & - \Delta\phi_{donnan,membrane/electrode} + \Delta\phi_{elec} \\ & + (\Delta\phi_d + \Delta\phi_{St})_{micropores},\end{aligned} \tag{5}$$

where all $\Delta\phi$'s are dimensionless voltage drops for different elements in the sub-cell: $\Delta\phi_{sp,half}$ is the voltage drop across half of the spacer channel (from the mid-plane to the edge, i.e. to the membrane), $\Delta\phi_{mem}$ is the voltage drop across the bulk of the membrane, $\Delta\phi_{donnan,membrane/spacer}$ and $\Delta\phi_{donnan,membrane/electrode}$ are Donnan potential drops at the interface between membrane and spacer, and between membrane and macropores in the electrode, respectively, which are given by Helfferich (1962), Ohki (1965), Vetter (1967).

$$\Delta\phi_{donnan} = \sinh^{-1}\frac{\omega X}{2c_{salt}}, \tag{6}$$

where $\Delta\phi_{donnan}$ is the Donnan potential for either of these two interfaces. In Eq. (6), the salt concentration is $c_{salt} = c_{spacer}$ when the interface between membrane and spacer channel is considered, and $c_{salt} = c_{mA}$ when taking the interface between membrane and the macropores in the electrode. Furthermore, in Eq. (6), ω is the sign of the membrane charge ($\omega = +1$ for an anion-exchange membrane), and X (with dimension mol/m^3) is the fixed membrane charge density. Furthermore, Eq. (5) shows the two contributions from the modified-Donnan EDL model, $\Delta\phi_d$ and $\Delta\phi_{St}$, calculated using Eqs. (1) and (2).

3.2. *Ion transport in membrane and in spacer channel*

In the flow direction, we discretize the spacer channel, as well as the electrodes, into M ideally-stirred volumes (or, sub-cells) placed in series, see Fig. 2. Starting with the spacer channel, for each volume, a salt mass balance is given by

$$\frac{\partial c_{sp,i}}{\partial t} = -\frac{J_{ion,i}}{\delta_{sp}} - \frac{M}{\tau_{sp}}\left(c_{sp,i} - c_{sp,i-1}\right), \tag{7}$$

where c_{sp} is the spacer channel salt concentration in mM = mol/m^3, i is the counter running from 1 to M, and τ_{sp} is the total spacer channel residence time (the spacer channel

volume, V_{sp}, divided by the spacer channel flow rate, Φ_{sp}). In Eq. (7), on the left-hand side is shown the accumulation term for salt, while the first term on the right-hand side gives the ion flux through one membrane (see Fig. 2) and the second term is the convective flow of salt from one sub-cell to the next. The effluent from cell i has concentration $c_{sp,i}$ (this is the stirred-volume approach) while the inflowing solution coming from the previous cell has concentration $c_{sp,i-1}$.

The current I, is discussed next. In each of the M volumes (or, sub-cells), the current I has the same value in the spacer channel, in the membrane, and in the electrode, but this value differs between sub-cells, and changes in time, also for CC operation (because only the average current, I_{tot}, is prescribed). For the spacer channel, the current relates to the electric potential difference across half of the spacer channel according to

$$I = -2D \cdot c_{sp} \cdot \frac{\Delta\phi_{sp,half}}{\delta_{sp}/2}. \tag{8}$$

Eq. (8) is valid when we assume that from membrane to membrane (across the width of the spacer channel) the salt concentration gradients are small. The diffusion coefficient in the spacer channel D can be taken as the average of that of the cation and the anion (Sonin and Probstein, 1968). For the membrane the current I relates to the inner-membrane potential drop, $\Delta\phi_{mem}$, and can be written as

$$I = -\frac{D_{mem}}{\delta_{mem}} \cdot \langle c_{T,mem} \rangle \cdot \Delta\phi_{mem}. \tag{9}$$

In this equation subscript "mem" is used for properties within the membrane and $c_{T,mem}$ is the total ion concentration in the membrane, given by $c_{T,mem} = c_{cation,mem} + c_{anion,mem}$. Furthermore, <…> denotes an average property and Δ is the difference across the membrane, while δ_{mem} is the membrane thickness. This equation is valid when the concentration $c_{T,mem}$ drops linearly across the membrane (Biesheuvel et al., 2011b). To solve the membrane model, we make use of the fact that at each position in the membrane, charge balance is maintained, given by $c_{cation,mem} - c_{anion,mem} + \omega X = 0$. In Eq. (9), D_{mem} is a diffusion coefficient of the ions within the membrane, assumed equal for cation and anion. Because of the locally high concentration of ions inside the membrane and because of its porous structure, the diffusion coefficient in the membrane, D_{mem} can be much lower than in the spacer channel (Andersen et al., 2012; Elattar et al., 1998).

At both solution/membrane edges, the total ion concentration in the membrane, $c_{T,mem}$, is given by $c_{T,mem} = 2 \cdot c_{salt} \cdot \cosh(\Delta\phi_{donnan}) = \sqrt{[X^2 + (2 \cdot c_{salt})^2]}$, with c_{salt} as for Eq. (6) either c_{sp} or c_{mA} (Biesheuvel, 2011). The average concentration $<c_{T,mem}>$ required in Eq. (9) is calculated as the average of these two boundary values for $c_{T,mem}$. The linearized ion flux through the membrane, J_{ion}, is given by

$$J_{ion} = -\frac{D_{mem}}{\delta_{mem}} (\Delta c_{T,mem} - \omega X \Delta\phi_{mem}). \tag{10}$$

3.3. Ion transport and storage in the electrode

Finally we describe the balance for total ion concentration in the electrode, relating to J_{ion}, by

$$\frac{\partial}{\partial t}\left(2 \cdot p_{mA} \cdot c_{mA,i} + p_{mi} \cdot \left(c_{cation,mi,i} + c_{anion,mi,i}\right)\right) = \frac{J_{ion,i}}{\delta_{elec}} + \frac{M}{\tau_{elec}}\left(c_{mA,i} - c_{mA,i-1}\right), \tag{11}$$

where τ_{elec} is the superficial residence time in the electrode (electrode total volume V_{elec} divided by the electrode flow rate Φ_{elec}). The total water flowrate per cell is Φ_{tot}, and the fraction of that which runs inadvertently through each of the electrodes is estimated as $\Phi_{elec} = \alpha \cdot \Phi_{tot}$, and thus $\Phi_{sp} = (1 - 2\alpha) \cdot \Phi_{tot}$. The effluents of the spacer channel and the two electrodes are combined into a single flow with the effluent salt concentration c_{eff} leaving the cell. It is the parameter c_{eff} which is measured, given theoretically by $c_{eff} = (1 - 2\alpha) \cdot c_{sp,M} + 2\alpha \cdot c_{mA,M}$. Theoretical predictions for this effluent salt concentration are presented in Fig. 4.

4. Results and discussion

In this section, we first discuss desalination cycles for CC operation of MCDI under the DSS condition and show the influence on a series of performance indicators, such as salt adsorption, charge transferred, and especially the average salt adsorption rate (ASAR) and water recovery (WR), by varying the following input parameters, namely: inflow salt concentration, adsorption current, water flowrate, desorption time, and desorption current. We will show the results for each parameter independently by varying each one in turn. In the second part of this section we describe results of CV operation of an MCDI system, focusing on the influence of cycle duration and desorption voltage. In all cases we compare experimental results with theoretical model predictions. An overview of the parameter settings for our theoretical calculations is presented in Appendix A.

4.1. Constant current (CC) operation of MCDI

4.1.1. Desorption in "zero volt desorption"-mode

In Section 4.1 we will present results of CC operation of MCDI in two operational modes: zero-volt desorption (ZVD) and reverse-current desorption (RCD).

Fig. 3 presents results for MCDI-CC-operation in ZVD mode, where the variation in effluent salt concentration during a single desalination cycle is shown. Both experimental and theoretical results are presented, and as can be observed all experiments can be well reproduced by the model. Fig. 3a shows that the duration of the desalination cycles depends on the influent salt concentration. For instance, when the influent salt concentration is decreased from 20 mM to 5 mM, the adsorption time drops from 200 s to only a couple of seconds. This can be explained by the fact that at lower influent concentrations we have a higher spacer resistance and quicker ion depletion. Therefore, at a fixed constant current of 1 A, the cell voltage reaches the set end voltage of 1.6 V much more rapidly.

In Fig. 3b and c it is shown that a lower effluent salt concentration can be achieved by increasing the electrical current during the adsorption step, as well as by decreasing the water flowrate. Fig. 3d shows that when we decrease the desorption time, the adsorption capacity per cycle decreases

and consequently the adsorption time also becomes shorter. This is because a decrease in the desorption time leads to incomplete release of counterions from the electrodes and consequently leads to a lower ion removal in the next adsorption step.

It can be observed in Fig. 3b and c that by varying the current during ion adsorption and/or by varying the water flowrate, the salt concentration in the effluent can either be increased or decreased, and therefore in the CC mode it is possible to fine-tune the salt concentration in the effluent water stream to a desired level (Zhao et al., 2012a).

Data such as obtained for the experiments shown in Fig. 3 are presented in aggregate form in Fig. 4 with each panel (a–d) in Fig. 3 corresponding to one column (I–IV) in Fig. 4. In Fig. 4 row A we present the total cycle time (t_{cycle}) and the water recovery (WR) as function of influent salt concentration (column I), adsorption current (column II), water flowrate (column III), and desorption time (IV). WR indicates the fraction of the salt stream which is reclaimed as freshwater. WR can be calculated according to:

$$WR = \frac{\Phi \cdot t_{ads}}{\Phi \cdot t_{ads} + \Phi \cdot t_{des}} = \frac{t_{ads}}{t_{cycle}} \quad (12)$$

where Φ is the water flowrate, t_{ads} the adsorption time, t_{des} the desorption time, and t_{cycle} is the sum of t_{ads} and t_{des}. As in our examples Φ is always the same for the adsorption and desorption step, we can use a simplified expression for WR ($=t_{ads}/t_{cycle}$).

Results of salt adsorption and charge per cycle are given in row B both experimentally and theoretically, as function of the same four parameters (column I–IV). Fig. 4B–I shows that when the influent salt concentration is increased from close to zero to around 20 mM, the salt adsorption and charge rapidly increase, but after that the salt adsorption again slightly decreases whereas the charge still increases. Fig. 4B-II shows that when the electrical current during adsorption is increased, both salt adsorption and charge decrease and when the electrical current is above 1.5 A, the decrease is even faster. Fig. 4B-III shows the existence of two regions, one of low charge and salt adsorption at a low flow rate $\Phi < 35$ mL/min, and one of high charge and salt adsorption for $\Phi > 35$ mL/min. All the experimental data can be reproduced very well with our theoretical model. However, some phenomena, for instance the rapid increase of salt adsorption when the influent salt concentration increases from zero to ~20 mM, or when the flowrate is increased beyond ~35 mL/min, do not have a single and easy explanation and must be due to the interplay of various process parameters.

For commercial use of an MCDI system it is important to have maximum salt removal within a given period of time. Therefore, in order to evaluate how quickly salt can be adsorbed, we introduce a new performance indicator, namely the average salt adsorption rate (ASAR) (see Fig. 4 row C), which is the salt adsorption per cycle, per gram of total electrode mass (Fig. 4-row B), divided by the cycle time (Fig. 4-row A). ASAR is a measure of the 'speed', or rate, of salt adsorption. The data in Fig. 4-row C demonstrate that when we vary each input parameter in turn, optimal values for ASAR are obtained in each case. The highest ASAR can be achieved at an influent salt concentration of around 20 mM (Fig. 4C-I), at an adsorption current of 1 A (Fig. 4C-II), at a water flowrate higher than 40 mL/min (Fig. 4C-III), and for a desorption time of 50 s (Fig. 4C-IV). Note that these optimized input parameters depend on the specific device, its operational mode, and values for other parameters. A general conclusion that can, however, be drawn is that the input parameter settings that lead to the highest salt adsorption per cycle do not always lead to the highest ASAR.

In addition, closer inspection of the results in Fig. 4 shows that for most cases, the trends in WR and ASAR as function of each input parameter are different. For instance, the highest ASAR can be achieved when the adsorption current of 1 A is used (Fig. 4C-II). However, for this condition the WR is less than 0.4 (Fig. 4A-II). Only when increasing the water flowrate, Φ, we find for the whole range of Φ simultaneously a higher ASAR and higher water recovery, see Fig. 4C-III.

In brief, we have demonstrated that in the CC-ZVD mode, variation of input parameters has a great impact on salt adsorption and electrical charge per cycle, and also on WR and ASAR, which are the two most important indicators to evaluate the performance of an MCDI system.

4.1.2. *Desorption in "reverse current desorption"-mode*

In a different operational mode, we apply a reversed current during desorption until V_{cell} becomes zero again (RCD mode).

Fig. 5a shows that by applying a less negative current during the desorption step, we extend the period of desorption and consequently also extend the duration of the adsorption step. This leads to more salt removal per cycle, see Fig. 5c. However, Fig. 5b shows that less negative desorption currents decrease the WR and increase the total cycle time. Combination of these effects is shown in Fig. 5d, where we show that as the desorption current becomes more negative, ASAR first increases and then decreases again. Thus, for this system, it is found that the highest ASAR is at a desorption current between −0.8 and −1.8 A, while the WR is highest at a desorption current of −2 A.

4.2. *Constant voltage (CV) operation of MCDI*

4.2.1. *Desorption in "zero volt desorption"-mode and in "reverse voltage desorption"-mode*

Next, we discuss CV operation of MCDI, which implies that during the adsorption step a constant voltage is applied, instead of a constant current. Constant Voltage (CV) is the classical operation mode of CDI and MCDI. CV operation can be done in the ZVD and the RVD mode, the difference to be discussed below. For all CV experiments, during salt adsorption a cell voltage of $V_{cell} = 1.2$ V is applied for a fixed period of time. During desorption in ZVD-mode we short-circuit the cell (i.e., apply $V_{cell} = 0$ V) for the same period. For the RVD-mode, we apply $V_{cell} = -1.2$ V (which is the reverse of the adsorption voltage) during desorption, also for the same period as adsorption. In both operational modes, because the water flowrate is the same in a complete cycle (60 mL/min for the full stack of $N = 8$ cells), and we set the adsorption time equal to the desorption time (both are half of the cycle time, which is varied in Fig. 6), the water recovery is always 50%. In Fig. 6 data for MCDI operation in CV-ZVD and CV-RVD mode are presented as function of cycle time. In Fig. 6(a) and (c), salt adsorption and charge per cycle per gram of total electrode mass are shown both experimentally and theoretically. As

Fig. 6 shows, when the cycle time exceeds 500 s, for both operational modes, salt adsorption and charge level off. However, ASAR peaks in both modes at a much shorter cycle time, around 200 s, indicating that in the present setup such a low cycle time of 200 s is the optimum value to achieve the highest ASAR (Fig. 6b and d).

4.2.2. *MCDI-CV operation with varying desorption voltage*

As can be inferred from Fig. 6a, c (similar to Fig. 4 in Biesheuvel et al., 2011a), by applying a negative cell voltage during desorption, it is possible to achieve about 20% more salt adsorption per cycle than simply by short-circuiting the cell during the desorption step, which is the classical operational mode of CDI and MCDI.

In order to find the optimal desorption voltage to achieve the maximum in ASAR, we performed a further series of CV experiments, where we vary the desorption voltage. An adsorption voltage of +1.2 V was applied for 500 s, and during desorption, the cell voltage was varied between 0 V and −2 V, also for a duration of 500 s. As the total cycle time for each experiment is 1000 s, ASAR follows the same trend as the salt adsorption per cycle shown in Fig. 7 and consequently is not shown. Both experimental data and results of theoretical calculations of salt adsorption and charge are presented in Fig. 7. It is observed that salt adsorption and charge increase slightly with desorption voltage, with for instance at a value of −1.4 V, approximately 20% more salt adsorption than for desorption at 0 V. However, at voltages more negative than −1.0 V, the charge per cycle increases strongly, which is not predicted by the model. For CDI, a similar observation was made when increasing the cell voltage during adsorption (Bouhadana et al., 2011). We believe the effect is due to Faradaic reactions, e.g. water splitting, at high desorption voltages. As a result, MCDI operated at very negative desorption cell voltages utilizes more charge, resulting in a less energy-efficient salt adsorption process, and is therefore not recommended.

4.3. *Discussion*

The interesting question is what can exactly be inferred from the data. Starting at Fig. 4, a comprehensive data set for MCDI-CC operation in the ZVD-mode is presented, focusing on the two key performance indicators for MCDI, namely water recovery (WR) and average salt adsorption rate (ASAR). As can be observed, varying influent salt concentration (column I), water flowrate (III), or desorption time (IV), in all cases leads to a similar trend in WR and in ASAR, both either going up or down with a change in one of the parameter settings. A difference is found in the dependence of ASAR and WR on the adsorption current (II), where the former has a maximum at an adsorption current around 1 A, while to achieve the highest WR, the adsorption current must be minimized.

Next, Fig. 5 summarizes data for MCDI-CC in the RCD-mode of operation. In this case we also find that ASAR and WR have a different dependency on the input parameter that is varied, being in this case the adsorption current, with ASAR being at

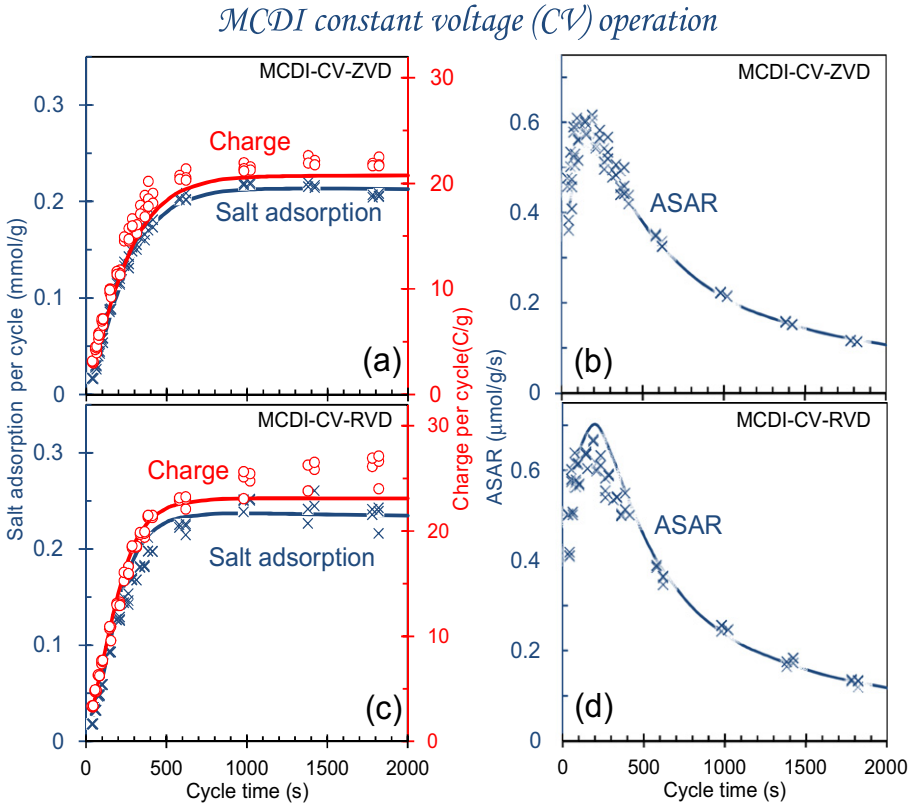

Fig. 6 – Experimental and theoretical results for MCDI-CV operation for ZVD and RVD mode. (a, c) Salt adsorption and charge. (b, d) Average salt adsorption rate (ASAR) in ZVD and RVD mode. For each experiment, during adsorption V_{cell} = 1.2 V, and during desorption V_{cell} = 0 V for ZVD and V_{cell} = −1.2 V for RVD. Periods of adsorption and desorption are the same, and the cycle time is the sum of these two. Lines: theory; symbols: experimental data.

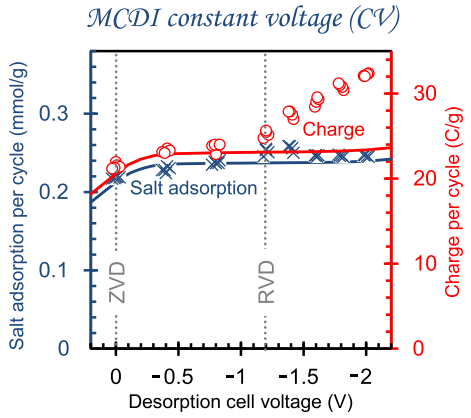

Fig. 7 – Salt adsorption and charge per gram of total electrode mass per cycle in MCDI-CV as function of negative desorption voltage (0 to −2 V). The desorption cell voltage is the cell voltage applied during the ion release-step. Other parameters to define the full cycle are: influent salt concentration $c_{salt,in}$ = 20 mM, durations of the adsorption and desorption step each 500 s, and voltage during adsorption V_{cell} = 1.2 V. Symbols: data; lines: theory. Symbols intersected by the dashed vertical lines correspond to the CV-ZVD and CV-RVD data at cycle time of 1000 s in Fig. 6.

a maximum in a fairly large range of values for the desorption current (between −0.8 and −1.8 A), while WR steadily increases with less negative desorption currents. The results for MCDI-CV (Figs. 6 and 7) demonstrate that optimum cycle times (to have the highest ASAR) are much shorter than typically considered in the literature (often beyond 10 min, approaching 1 h); here we find a maximum ASAR at a cycle time of only 200 s, much shorter than previously used values. All of these results show that the complete optimization of an MCDI system, considering also energy costs and material properties, is a complicated task requiring multidimensional optimization.

In general, Figs. 3–7 show that our two-porosity modified-Donnan model well describes the data when we fit the CV-data and CC-data separately using as freely adjustable parameters the membrane charge density X, the ion diffusion coefficient in the membrane D_{mem}, the fraction of the total water flow going through one electrode, α, as well as the specific electrode resistance, R_{elec}. However, as may be observed from Table A in Appendix A, to fit these two large data sets (one for CV- and the other for CC-operation), we need to use different numbers for X, D_{mem} and α. This is not an optimal situation and indicates that our model is not yet fundamentally rigorous, because ideally one set of model parameters describes data both for CC and CV operation at the same time. Several model improvements can be made to help us achieve this aim, as summarized next: first of all, full porous electrode theory has not yet been implemented, but instead we have assumed that in each sub-cell we have equalized properties across the electrode, with the ionic resistance empirically described by a single parameter R_{elec}. An improved model makes use of porous electrode theory and does not need this parameter R_{elec}. Secondly, for the membrane we have assumed equal ion diffusion coefficients for the counterion and the co-ion. However, as known from membrane open-circuit voltage diffusion potential measurements (Barragán et al., 2009), the co-ion can have a different mobility (diffusion coefficient) from the counterion. This effect can be included in an improved model. Furthermore, at the moment the spacer channel is modelled as a series of stirred tanks, and the exact concentration profile of ions across the channel (in the direction from membrane to membrane) is not yet considered. Finally, our model assumes perfect symmetry of anode and cathode, which is not true in reality because the cation and anion have different diffusion coefficients (both in the open space, and in the membranes), and because the anion-exchange membrane and the cation-exchange membrane have a different charge density. When all of these effects are included in a full-scale model, it is hopefully possible to fit all presented data sets in this work by one and the same model, with one set of input parameters. Such a model can be confidently used for process optimization studies.

5. Conclusions

In this work we have presented experimental and theoretical results for CC and CV operation in the membrane capacitive deionization (MCDI) process. We have systematically varied the following input parameters, namely influent salt concentration, water flowrate, adsorption and desorption current, desorption voltage, and adsorption and desorption times, and presented their effect on salt adsorption per cycle, total charge, and water recovery (WR). We define the average salt adsorption rate (ASAR) to evaluate the rate of desalination, and demonstrate a systematic procedure to optimize the input parameters in order to reach the highest ASAR. A theoretical MCDI process model is validated by comparison with experimental data, with the outcome that in most cases the theory describes the experimental results very well, though the need for parameter settings that differ between CC and CV operation makes it clear that the model must be significantly improved. In the future, an exact optimization of parameter settings can be realized based on a validated MCDI process model, in order to obtain the highest ASAR and WR for the operation of a particular MCDI system.

Acknowledgements

This work was performed in the TTIW-cooperation framework of Wetsus, Centre of Excellence for Sustainable Water Technology. Wetsus is funded by the Dutch Ministry of Economic Affairs, the European Union Regional Development Fund, the Province of Friesland, the City of Leeuwarden, and the EZ/Kompas program of the 'Samenwerkingsverband Noord-Nederland'. We thank the participants of the theme "Capacitive Deionization" for their involvement in this research.

Appendix A. Parameter setting

In appendix A we summarize all the parameter settings required for comparing the model to the data given in the figures throughout the results and discussion section.

Appendix B. Electrical circuit analogue of MCDI system

In appendix B we present a schematic diagram of the electric circuit analogue of the MCDI system, see Fig. B. To avoid the numerical problem that occurs when we apply a step change in current to the MCDI cell, we have placed a very small capacitance in the external circuit, $C_{cap} = 2$ mF/m^2, parallel to the MCDI cell, so the applied electrical current, I_{max}, will first saturate the small capacitor and then charge the system with current I_{tot}, according to

$$\frac{\partial V_{cell}}{\partial t} = F \cdot \frac{I_{max} - I_{tot}}{C_{cap}}. \quad (13)$$

Initially, because of the spacer channel resistance, all the applied current, I_{max}, goes to the external capacitor, thus initially the current to the MCDI cell will be zero, $I_{tot} = 0$. However, in time, when the external capacity saturates, I_{cap} becomes zero, and the average current into the MCDI cell, I_{tot}, will approach the value of I_{max}. Note that in the model I_{tot} distributes self-consistently over the M numerical sub-cells, see Fig. 2. Another method to avoid the numerical discontinuity after each sudden change in current (at time t^*) is to solve jointly Eqs. (4), (5), (8) and (9) for all sub-cells 1…M, together with $I_{tot} = 1/M \sum_{i=1}^{M} I_i$, with $\Delta\phi_{donnan}$ and $(\Delta\phi_d + \Delta\phi_{St})_{mi}$ in each sub-cell unvarying at t^*, to calculate in this way the cell voltage and currents I_i right after t^*.

Table A – Parameter settings for theoretical MCDI transport model. Numbers with subscripts *cc* are for constant current operation (Figs. 3–5) and subscripts *cv* denote constant voltage operation (Figs. 6 and 7).

Symbols		Value	Dimension
p_{mA}	Porosity of macropores	0.30	
p_{mi}	Porosity of micropores	0.30	
$C_{St,vol,0}$	Volumetric Stern layer capacitance (low charge limit)	0.12	GF/m^3
α	Parameter to describe non-linear part of Stern capacity	17.3	F m^3/mol^2
R_{elec}	Specific electrode resistance	0.12_{cc} 0.108_{cv}	Ω mol/m
X	Fixed membrane charge density	3000_{cc} 8000_{cv}	mol/m^3
D	Ion diffusion coefficient in the spacer channel	1.68	10^{-9} m^2/s
D_{mem}	Ion diffusion coefficient in the membrane	1.12_{cc} 0.168_{cv}	10^{-9} m^2/s
V_{sp}	Total volume of one spacer channel	0.147	mL
V_{elec}	Total volume of one electrode	0.153	mL
α	Fraction of total flow going through one electrode	1 %$_{cc}$ 0.25 %$_{cv}$	
μ_{att}	Chemical attraction term between ions and carbon	1.4	kT
M	Number of sub-cells in the model	6	
C_{cap}	Capacitance in the external circuit	2	mF/m^2

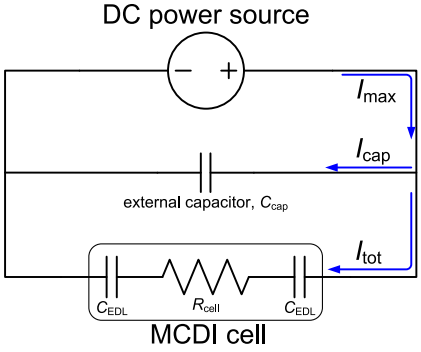

Fig. B – Electrical circuit analogue for MCDI cell combined with external capacity. Here, I_{max} is the constant applied electrical current, part of which, I_{cap}, will be used to charge the external capacitor, C_{cap}, which represents external wires and connections. I_{tot} depicts the electrical current going into the MCDI cell, C_{EDL} represents the electric double layer capacitance, and R_{cell} represents the cell resistance.

REFERENCES

Andersen, M.B., van Soestbergen, M., Mani, A., Bruus, H., Biesheuvel, P.M., Bazant, M.Z., 2012. Current-induced membrane discharge. Physical Review Letters 109 (10), 108301.

Anderson, M.A., Cudero, A.L., Palma, J., 2010. Capacitive deionization as an electrochemical means of saving energy and delivering clean water. Comparison to present desalination practices: will it compete? Electrochimica Acta 55 (12), 3845–3856.

Arnold, B.B., Murphy, G.W., 1961. Studies on electrochemistry of carbon and chemically modified carbon surfaces. Journal of Physical Chemistry 65 (1), 135.

Avraham, E., Noked, M., Cohen, I., Soffer, A., Aurbach, D., 2011. The dependence of the desalination performance in capacitive deionization processes on the electrodes PZC. Journal of the Electrochemical Society 158 (12), P168–P173.

Barragán, V.M., Villaluenga, J.P.G., Godino, M.P., Izquierdo-Gil, M.A., Ruiz-Bauzá, C., Seoane, B., 2009. Experimental estimation of equilibrium and transport properties of sulfonated cation-exchange membranes with different morphologies. Journal of Colloid and Interface Science 333 (2), 497–502.

Biesheuvel, P.M., Fu, Y., Bazant, M.Z., 2011a. Diffuse charge and Faradaic reactions in porous electrodes. Physical Review E 83 (6), 061507.

Biesheuvel, P.M., Zhao, R., Porada, S., van der Wal, A., 2011b. Theory of membrane capacitive deionization including the effect of the electrode pore space. Journal of Colloid and Interface Science 360 (1), 239–248.

Biesheuvel, P.M., 2011. Two-fluid model for the simultaneous flow of colloids and fluids in porous media. Journal of Colloid and Interface Science 355 (2), 389–395.

Biesheuvel, P.M., Fu, Y., Bazant, M.Z., 2012. Electrochemistry and capacitive charging of porous electrodes in asymmetric multicomponent electrolytes. Russian Journal of Electrochemistry 48 (6), 580–592.

Bouhadana, Y., Ben-Tzion, M., Soffer, A., Aurbach, D., 2011. A control system for operating and investigating reactors: the demonstration of parasitic reactions in the water desalination by capacitive de-ionization. Desalination 268 (1–3), 253–261.

Buerkle, T., 14 Feb. 2007. Making Every Drop Count. http://www.fao.org/newsroom/en/news/2007/1000494/index.html.
Cipollina, A., 2009. Seawater Desalination: Conventional and Renewable Energy Processes. Springer, Berlin.
Elattar, A., Elmidaoui, A., Pismenskaia, N., Gavach, C., Pourcelly, G., 1998. Comparison of transport properties of monovalent anions through anion-exchange membranes. Journal of Membrane Science 143 (1–2), 249–261.
Haro, M., Rasines, G., Macias, C., Ania, C.O., 2011. Stability of a carbon gel electrode when used for the electro-assisted removal of ions from brackish water. Carbon 49 (12), 3723–3730.
Helfferich, F.G., 1962. Ion Exchange. Dover.
Humplik, T., Lee, J., O'Hern, S.C., Fellman, B.A., Baig, M.A., Hassan, S.F., Atieh, M.A., Rahman, F., Laoui, T., Karnik, R., Wang, E.N., 2011. Nanostructured materials for water desalination. Nanotechnology 22 (29), 292001.
Kim, Y.-J., Hur, J., Bae, W., Choi, J.-H., 2010. Desalination of brackish water containing oil compound by capacitive deionization process. Desalination 253 (1–3), 119–123.
Kim, Y.-J., Choi, J.-H., 2010. Improvement of desalination efficiency in capacitive deionization using a carbon electrode coated with an ion-exchange polymer. Water Research 44 (3), 990–996.
Lee, J.-B., Park, K.-K., Eum, H.-M., Lee, C.-W., 2006. Desalination of a thermal power plant wastewater by membrane capacitive deionization. Desalination 196 (1–3), 125–134.
Lee, J.-Y., Seo, S.-J., Yun, S.-H., Moon, S.-H., 2011. Preparation of ion exchanger layered electrodes for advanced membrane capacitive deionization (MCDI). Water Research 45 (17), 5375–5380.
Li, H., Gao, Y., Pan, L., Zhang, Y., Chen, Y., Sun, Z., 2008. Electrosorptive desalination by carbon nanotubes and nanofibres electrodes and ion-exchange membranes. Water Research 42 (20), 4923–4928.
Li, H.B., Zou, L., 2011. Ion-exchange membrane capacitive deionization: a new strategy for brackish water desalination. Desalination 275 (1–3), 62–66.
Nie, C.Y., Zhan, Y.K., Pan, L.K., Li, H.B., Sun, Z., 2011. Electrosorption of different cations and anions with membrane capacitive deionization based on carbon nanotube/nanofiber electrodes and ion-exchange membranes. Desalination and Water Treatment 30 (1–3), 266–271.
Ohki, S., 1965. Rectification by a double membrane. Journal of the Physical Society of Japan 20 (9), 1674–1685.
Park, B.-H., Kim, Y.-J., Park, J.-S., Choi, J., 2011. Capacitive deionization using a carbon electrode prepared with water-soluble poly(vinyl alcohol) binder. Journal of Industrial and Engineering Chemistry 17 (4), 717–722.
Porada, S., Sales, B.B., Hamelers, H.V.M., Biesheuvel, P.M., 2012a. Water desalination with wires. The Journal of Physical Chemistry Letters 3 (12), 1613–1618.
Porada, S., Weinstein, L., Dash, R., van der Wal, A., Bryjak, M., Gogotsi, Y., Biesheuvel, P.M., 2012b. Water desalination using capacitive deionization with microporous carbon electrodes. ACS Applied Materials & Interfaces 4 (3), 1194–1199.
Porada, S., Bryjak, M., van der Wal, A., Biesheuvel, P.M., 2012c. Effect of electrode thickness variation on operation of capacitive deionization. Electrochimica Acta 75, 148–156.
Rica, R.A., Brogioli, D., Ziano, R., Salerno, D., Mantegazza, F., 2012. Ions transport and adsorption mechanisms in porous electrodes during capacitive-mixing double layer expansion (CDLE). The Journal of Physical Chemistry C 116 (32), 16934–16938.
Seo, S.-J., Jeon, H., Lee, J.K., Kim, G.-Y., Park, D., Nojima, H., Lee, J., Moon, S.-H., 2010. Investigation on removal of hardness ions by capacitive deionization (CDI) for water softening applications. Water Research 44 (7), 2267–2275.
Sonin, A.A., Probstein, R.F., 1968. A hydrodynamic theory of desalination by electrodialysis. Desalination 5 (3), 293–329.
Suss, M.E., Baumann, T., Bourcier, B., Spadaccini, C., Rose, K.A., Santiago, J.G., Stadermann, M., 2012. Capacitive desalination with flow-through electrodes. Energy & Environmental Science 5, 9511–9519.
Vetter, K.J., 1967. Electrochemical Kinetics. Academic Press.
Zhao, R., Biesheuvel, P.M., van der Wal, A., 2012a. Energy consumption and constant current operation in membrane capacitive deionization. Energy & Environmental Science 5, 9520–9527.
Zhao, R., Biesheuvel, P.M., Miedema, H., Bruning, H., van der Wal, A., 2010. Charge efficiency: a functional tool to probe the double-layer structure inside of porous electrodes and application in the modeling of capacitive deionization. The Journal of Physical Chemistry Letters 1 (1), 205–210.
Zhao, R., van Soestbergen, M., Rijnaarts, H.H.M., van der Wal, A., Bazant, M.Z., Biesheuvel, P.M., 2012b. Time-dependent ion selectivity in capacitive charging of porous electrodes. Journal of Colloid and Interface Science 384 (1), 38–44.
Zou, L., Li, L., Song, H., Morris, G., 2010. Improving the capacitive deionisation performance by optimising pore structures of the electrodes. Water Science and Technology 61 (5), 1227–1233.